Aeolian Research 19 (2015) 55–63

Contents lists available at ScienceDirect

Aeolian Research

journal homepage: www.elsevier.com/locate/aeolia

Variability of magnetic character of S5-1 paleosol (age ~470 Ka) along a rainfall transect explains why susceptibility decreased with high rainfall

Xuelian Guo [a,b,*], Xiuming Liu [c,d], Shengjun Miao [e], Guoyong Zhao [f], Yixin Liu [a]

[a] School of Earth Sciences, Key Laboratory of Western China's Mineral Resources of Gansu Province, Lanzhou University, Lanzhou 730000, China
[b] Institute for Rock Magnetism, University of Minnesota, Twin Cities, Minneapolis 55414, USA
[c] Research Centre of Global Change, School of Geographical Science, Fujian Normal University, Fuzhou 350007, China
[d] Department of Environment and Geography, Macquarie University, NSW 2109, Australia
[e] School of Civil and Environmental Engineering, University of Science and Technology Beijing, Beijing 100083, China
[f] College of Urban and Environmental Science, Xinyang Normal University, Xinyang 464000, China

ARTICLE INFO

Article history:
Received 13 February 2015
Revised 2 September 2015
Accepted 4 September 2015
Available online 27 September 2015

Keywords:
Magnetic characters
Magnetic alteration
S5-1 paleosol
CLP

ABSTRACT

This study was based mainly on environmental magnetic, soil science and geochemical methods to analyze the spatial variation of magnetic characteristics of the S5-1 paleosol (age ~470 Ka) in a NW–SE transect from Xifeng, Linyou and Baoji sections from the Chinese Loess Plateau. The results show that (a) pedogenesis and chemical weathering of the coeval S5-1 paleosol layers increased with rainfall from Xifeng to Baoji, (b) the proportion of the pedogenic maghemite component decreased, while (c) the concentrations of weakly magnetic antiferromagnetic minerals (hematite and goethite) relatively increased. Maghemite and hematite appear to have formed simultaneously with development of pedogenesis, thus being similar in this aspect to soil in arid regions of SW Spain. However, amount of goethite did not show a consistent relationship as observed from magnetism in the three sections. Maghemite was found to be the main contributor to magnetic enhancement. Iron–manganese cutans, an indicator of diagnesis, increased with the rainfall in the S5-1 paleosol layer from Xifeng to Baoji. As expected, they show that pedogenesis occurred intermittently between wet and dry conditions causing iron mineral transformation. However, we suggest that parts of the fine-grained strongly magnetic minerals (mainly oxidized magnetite and maghemite) were converted into weakly magnetic minerals (mainly hematite and goethite) by pedogenesis, which resulted in a decline in the finest superparamagnetic (SP) and stable single-domain (SSD) ferrimagnetic minerals, thus decreasing the susceptibility of S5-1 paleosol from north to south. This behavior in a high rainfall region is different from the aerobic soil in SW Spain in which part of the initial hydro-maghemite transformed only to hematite rather than goethite and hematite.

1. Introduction

Over the past 20 years, the relation between magnetic enhancement and rainfall has been systematically investigated over Chinese loess deposits. However, the relationships between soil magnetic susceptibility and pedogenesis in different regions are different. Magnetic susceptibility shows a generally positive correlation with pedogenic intensity in the central Chinese Loess Plateau (CLP), such as Xifeng (Liu et al., 2001), Lingtai (Ding et al., 1998) and Luochuan (Balsam et al., 2004). In the Xinjiang region, however, there is a more complex correlation between magnetic susceptibility and pedogenesis. Furthermore, globally different explanations of the mechanism of susceptibility enhancement have been proposed (Song et al., 2010; Guo et al., 2011; Orgeira et al., 2011). In addition, magnetic susceptibility of the loess profiles in Siberia and Alaska demonstrate a lower susceptibility in paleosols due to aridity. This latter phenomenon is explained by the increased transport of magnetite due to strong activity of "wind vigor" during the glacial periods (Begét et al., 1990; Evans et al., 2003; Chlachula, 2003; Lagroix and Banerjee, 2004; Kravchinsky et al., 2008), or water logging and reducing conditions in permafrost layers which led to the chemical transformation of wind-blown ferromagnetic minerals and the reduction in magnetic susceptibility in paleosols (Bábek et al., 2011; Taylor and Lagroix, 2014).

Previous studies have proposed various explanations about loess–paleosol susceptibility enhancement mechanism. But it is

* Corresponding author at: School of Earth Sciences, Key Laboratory of Western China's Mineral Resources of Gansu Province, Lanzhou University, Lanzhou 730000, China.

http://dx.doi.org/10.1016/j.aeolia.2015.09.003
1875-9637/

now generally accepted that neoformed fine-grained magnetite and maghemite, generated in situ by inorganic or perhaps microbial pedogenesis, have increased the paleosol susceptibility (Zhou et al., 1990; Banerjee et al., 1993; Hunt et al., 1995; Fine et al., 1995; Maher, 1998; Deng et al., 2001; Porter et al., 2001; Spassov et al., 2003; Qiang et al., 2005; Xie et al., 2009).

According to recent rock magnetic and mineralogical models, fine-grained pedogenic maghemite play a key role in determining increase or decrease of susceptibility (Liu et al., 2005, 2007; Nie et al., 2010). However, Torrent et al. (2007, 2010) has suggested that under some contains, especially in Spain, hydro-maghemite causes the magnetic enhancement. Pedogenic maghemite has a distribution of grain sizes comprised between 10 and 100 nm and therefore happens to include mainly SP and SD domain states, with very minor addition of larger PSD particles (Liu et al., 2007; Geiss and Zanner, 2006). In limited areas understanding the basis of susceptibility mechanism has greatly promoted quantitative recovery of paleoclimatic indicators (rainfall and temperature) (Liu et al., 1995; Maher et al., 2003). As a valuable climatic proxy from Chinese loess deposits, magnetic susceptibility has been used for quantitative reconstruction of precipitation (Heller et al., 1993; Liu et al., 1995; Han et al., 1996; Hao and Guo, 2005; Balsam et al., 2011), although there is still no agreement about exact precipitation values from the different reconstructions.

Spatial variations of chemical weathering and decreasing trend of paleo-weathering in both paleosol and loess units from southeast to northwest in CLP are consistent with the modern rainfall pattern (Hao and Guo, 2005). The S5 layer is the most prominent and well-developed paleosol unit in CLP. The S5 period represents a climatic optimum during the past 2.5 Ma (An et al., 1987). In general, the paleosol sub-unit S5-1 has the highest or near highest susceptibility value in the central CLP thus representing highest temperature and humidity. However, in the southern CLP, precipitation is more abundant than the central of CLP, yet magnetic susceptibility value of S5-1 layer is not the highest (Kalm et al., 1996; Zhao et al., 2013; Guo et al., 2013). In the work presented here we have attempted a quantitative explanation of this anomaly.

Our work involves paleosol S5-1 (age from 0.448 to 0.479 Ma; Willimas et al., 1993) that has been sampled along a nearly north–south transect from Xifeng to Baoji along which mean annual rainfall (MAR) increases from 550 to 720 mm/y. The parent material is loess or aeolian dust which originated in north-west China and was deposited everywhere in the CLP. Thus, we expected the susceptibility of the S5-1 horizon to show the known positive relationship between MAR and susceptibility. Furthermore, since MAR is highest in our sampling site in the southernmost site, 720 mm/y, we hoped be able to test the models of Orgeira et al. (2011), Maher and Thompson (1994), and Han et al. (1996) that predict magnetic enhancement declining when rainfall or precipitation–evaporation reaches a critical high value.

Ferrimagnetic magnetite and its low-temperature oxidation product, loosely called 'maghemite' are mainly responsible for magnetic enhancement. According to soil effective moisture's models (Orgeira et al., 2011), the variations in the alternation under strongly oxidizing and reducing conditions should lead to 'maghemite' formation and magnetic enhancement initially. Qualitatively, then 'maghemite' may gradually decrease under reducing condition (Maher, 1998; Hanesch and Scholger, 2005; Fischer et al., 2008), and finally convert into weakly magnetic goethite etc., which greatly reduce susceptibility in paleosols. The hypothesis we propose to test with a rainfall transect is that under seasonal abundant rainfall, when iron is reduced from ferric to ferrous ions due to lower pH, we should observe a drop in susceptibility after a critical rainfall value is reached in our study transect. Thus we hoped to observe, after the critical value of MAR, susceptibility in this transect is no longer a reliable indicator of past MAR. In addition, we will use geochemical analysis and description of soil properties in addition to magnetic data to elucidate the origin of any observed susceptibility variation. In particular, our conclusion may shed light on the complex unresolved relationship between magnetic susceptibility and pedogenesis especially around the southern edge of the CLP.

2. Samples and measurements

2.1. Sampling

Three paleosol sections were sampled at 5 cm intervals from the bottom of L5 loess through S5 paleosol layer down to the top of the L6 loess layer of CLP (Fig. 1). Xifeng (XF) (35°46′N, 107°41′E) is located in the central CLP. Baoji (BJ) (34°25′N, 107°07′E) is located about 260 km south from XF on the southern edge of the CLP, at the north 'foot' of the Qinling Mountains. Linyou (LY) (34°45′N, 107°49′E) is located between the two sites on the southeast of XF section, and to the northeast of BJ. The present climate of the area is semi-arid, mildly humid with the mean annual rainfall (MAR) of 550, 680, and 720 mm (up to 1100 mm in Qinling Mountain area) from XF to LY to BJ, respectively (Fig. 1). Sixty percent of precipitation occurs from July to September. The mean annual temperatures (MAT) are 8.7, 9.1 and 12 °C, respectively. Precipitation is carried by the south east summer monsoon, which decreases from south (BJ) to north (XF). Most of the samples for study were collected from S5 paleosols layers along with loess boundaries at the XF, LY and BJ sections.

2.2. Magnetic measurements and geochemical analysis

The samples were air-dried, then weighed and packed in a nonmagnetic plastic box (2 × 2 × 2 cm). Magnetic susceptibility (χ, mass-specific) was measured using Bartington MS-2 meter (low frequency χ_{lf} with 470 Hz, high frequency χ_{hf} with 4700 Hz). The frequency-dependent susceptibility was calculated as follows: $\chi_{fd} = \chi_{lf} - \chi_{hf}$. Low-temperature susceptibility was measured using a Kappabridge KLY-3S low temperature system (from −200 to 0 °C), using about 0.4 g of each sample. Anhysteretic remanent magnetization (ARM) was measured in a Minispin Magnetometer after magnetization with a DTECH AF demagnetizer. The peak alternating field (AF) field used was 100 mT and the DC bias was

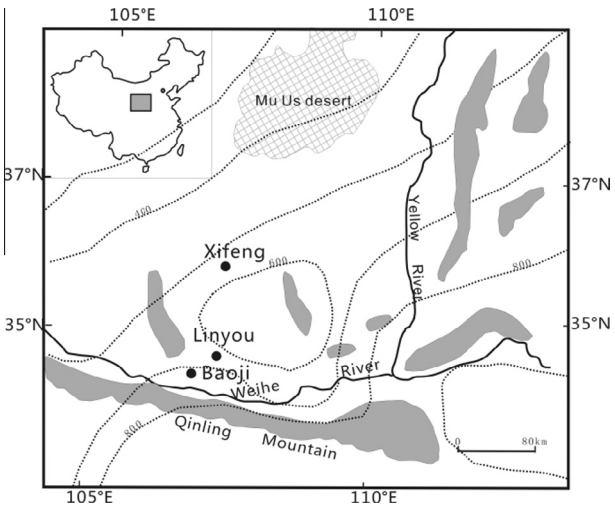

Fig. 1. Map showing the study sites. Also shown are the deserts (reticulated) and mountains (gray) around and within the CLP.

50 μT. ARM was then normalized by the bias field to obtain ARM susceptibility (χ_{ARM}). Afterwards isothermal remanent magnetization (IRM) was acquired in progressively increasing magnetic fields up to 1T with a MMPM 10 pulse magnetizer and the induced remanence after each field was measured in the Minispin Magnetometer. The IRM acquired in the maximum field of 1T was defined as the saturation isothermal remanent magnetization (SIRM = IRM_{1T}). Hysteresis loops were measured using a Princeton Measurements Vibrating Sample Magnetometer (VSM). From the hysteresis loops, saturation magnetization (M_s), saturation remanence magnetization (M_{rs}), coercivity (B_c), remanent coercivity (B_{cr}), antiferromagnetic content (HIRM or 'hard' IRM) and ferrimagnetic content (S_{300}) were determined. A Quantum Design MPMS-2 superconducting quantum interference device (SQUID) magnetometer was used to perform measurements of cooling curves of RT (room temperature) remanence (SIRM) cooling curves and also for Zero Field Cooled (ZFC) remanence curves. For ZFC experiment SIRM was imparted by a 2.5 T field at 300 K; Samples were then cooled in zero field down to 20 K in 5 K steps and were warmed back to room temperature in zero field.

The visible diffuse reflectance spectra (DRS), specifically measures the redness (a) and lightness (L) in color obtained over the range from 400 to 700 nm wavelengths at 2 nm intervals using a Perkin Elmer Lambda 950 spectrophotometer. The method of Torrent et al. (2007) was used to derive the second-order derivative of the Kubelka–Munk remission spectrum. The intensities of the bands at ~425 nm (I_{425}) and ~535 nm (I_{535}) are proportional to the concentration of goethite and hematite, respectively (Scheinost et al., 1998), and can be used as proxies for relative changes in the mass concentration of goethite and hematite (Torrent et al., 2007; Zhang et al., 2012). Allowing calculation of hematite and goethite in the studied paleosol samples. Root Mean Square error (RMSE) for hematite is 0.0596, and for goethite estimation RMSE is 0.1714 (Zhang et al., 2009).

Elements K_2O, Na_2O, CaO, Fe_2O_3, Al_2O_3, SiO_2 and Rb concentrations were measured using XRF spectrography. For each XRF measurement, a 4 g whole-rock sample was powdered in agate mortar, sieved to a size-fraction of <200 mesh, and then compacted into a round disk and measured with a VP-320 XRF spectrometer made in Japan. The relative standard deviation is about 1%, and the relative errors estimated from the measured values and the recommended values for the standards are less than 2%. The free Fe_2O_3 (FeD) was extracted by the citrate-bicarbonate-dithionite (CBD) method and total Fe_2O_3 (FeT) was analyzed on completely acid-dissolved samples, both being measured on a WFD-Y2 atomic adsorption unit.

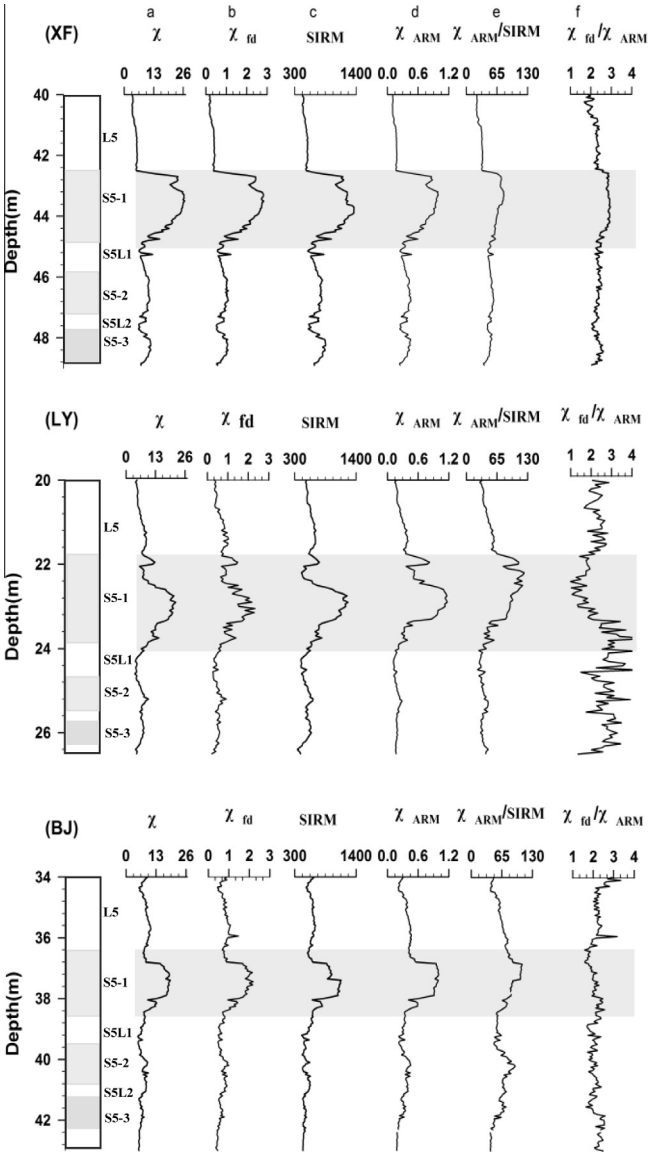

Fig. 2. Magnetic parameters of S5 paleosols at XF, LY and BJ sections. The units of the above parameters are expressed in units of χ (a): 10^{-7} m^3 kg^{-1}; χ_{fd} (b): 10^{-7} m^3 kg^{-1}; SIRM (c): 10^{-5} Am^2 kg^{-1}; χ_{ARM} (d): 10^{-5} m^3 kg^{-1}; χ_{ARM}/SIRM (e): 10^{-5} mA^{-1}; χ_{fd}/χ_{ARM} (f).

3. Results

3.1. Spatial and depth variation of magnetic properties of S5-1 paleosol

Magnetic susceptibility is controlled mainly by magnetic mineral composition, concentration, and grain size. In general, the maximum χ value of paleosol S5-1 is seen to decrease from XF to LY to BJ (Fig. 2a and Table 1). It can be seen that the χ value of BJ S5-1 paleosol unit (highest rainfall) is the lowest in all three sections, and also lower by about a factor of two than the relatively weak pedogenic S3 horizon (maximum value of 36.75×10^{-7} m^3 kg^{-1}) higher up in the same section (Guo et al., 2013).

χ_{fd} is proportional to the concentration of the viscous SP particles (Worm, 1998). The maximum χ_{fd} value displays a decreasing trend from XF to LY to BJ (Fig. 2b and Table 1), indicating that SP grains also reduce. The same trend observed with χ reflects that SP grains is the main contributor to χ in S5-1 paleosol unit.

SIRM is dominated by the composition and concentration of the larger particles of ferrimagnetic minerals. If the mineral compositions are the same, SIRM reflects the concentration of non-SP and mainly the larger (MD, >10 μm) ferrimagnetic minerals in samples. The maximum SIRM value of S5-1 unit decreases from XF, LY to BJ (Fig. 2c and Table 1), indicating that concentration of the larger particles of ferrimagnetic minerals in S5-1 layers also decrease from north to south.

χ_{ARM} and χ_{ARM}/SIRM ratios can help determine the identity of magnetic particles and the small grain size fractions. χ_{ARM} is extremely sensitive to non-interacting SD particles. χ_{ARM}/SIRM expresses the ratio between (non-interacting) SD particles and total ferrimagnetic contributions from all particles (Banerjee et al., 1981; King et al., 1982). Contrary to χ and χ_{fd}, χ_{ARM} and χ_{ARM}/SIRM do not show a monotonic trend from XF to BJ (Fig. 2d and e). It increases from XF to LY and then decreases from LY to BJ, a possible reason may be related to grain size variations. The ratio χ_{fd}/χ_{ARM} can be used to quantify the finest grain size of χ and ARM carriers (King et al., 1982; Liu et al., 2004). The positive correlation between χ_{fd}/χ_{ARM} and χ_{fd} of XF S5-1 unit (Fig. 2f) indicate the increasing influence of SP particles that only can

Table 1
The maximum values of the magnetic parameters in S5-1 units at XF, LY and BJ sections.

Sections	χ (10^{-7} m^3 kg^{-1})	χ_{fd} (10^{-7} m^3 kg^{-1})	SIRM (10^{-5} Am^2 kg^{-1})	χ_{ARM} (10^{-5} m^3 kg^{-1})	χ_{ARM}/SIRM (10^{-5} mA^{-1})	χ_{fd}/χ_{ARM}
XF S5-1	26.36	2.83	1336	0.99	87.21	2.88
LY S5-1	21.12	2.33	1240	1.66	122.94	2.18
BJ S5-1	18.73	2.15	1130	1.17	108.42	2.22

contribute to χ_{fd} (Liu et al., 2004). In contrast, there is a clearly negative correlation in LY S5-1 unit and an imprecise negative correlation in BJ S5-1 unit in Fig. 2f. It indicates that there is variability in grain-size distributions despite the increase in the concentration of the χ_{fd} and χ_{ARM} carriers, confirming the inconsistent trend shown by χ_{ARM} and χ_{ARM}/SIRM from XF to BJ.

The low-temperature remanence curves can provide estimates of low temperature oxidation from the shapes of heating and cooling of SIRM curves (Özdemir and Dunlop, 2010). For RTSIRM (300 K isothermal remanence) on cooling (Fig. 3a), the SIRM at first increases linearly from 300 K, showing either an increase in M_s or decrease in superparamagnetic behaviors, but when approaching the Verwey transition of magnetite, the asymmetric humped shapes of RT remanence curves are indicative of low temperature oxidation or partial 'maghemitization' (Özdemir and Dunlop, 2010). The degree of maghemitization appears to increase from XF to LY to BJ. The weak crystallographic Verwey transitions (Tv) in remanence at about 120 K indicate the existence of slightly oxidized magnetite in three samples.

In ZFC remanence curves (Fig. 3b), the paleosol S5 all display SP contribution. But BJL6 sample curve from underlying loess sample with sharp and steep Verwey transition at about 120 K shows that it has the smallest SP grains. The other three paleosol curves, without obvious Verwey transition at about 120 K, show that grain sizes are more oxidized and finer, and they display the presence of more SP grains in paleosols than in parent loess (BJL6 sample). In contrast, SP fraction are nearly similar for XF and LY samples, but higher than the BJ S5 sample, thus showing a small drop in SP% at BJ.

The shape of hysteresis loops can qualitatively indicate magnetic mineral compositions (Evans and Heller, 2003). Three magnetically separated representative samples (Fig. 4) show that the open hysteresis loops below 300 mT are closed above 300 mT, indicating that they contain softer magnetic minerals (magnetite and/or 'maghemite'). However, all three loops remained unsaturated above 300 mT, suggesting that high-coercivity hard magnetic minerals, such as goethite and/or hematite, are present in all these samples (Guo et al., 2011). The hysteresis parameters M_{rs}, B_c, B_{cr} increase monotonically from XF to BJ (Fig. 4) pointing to increase in high coercivity mineral such as hematite or goethite, or it could also indicate increase in SD magnetite/maghemite. The wasp-waisted hysteresis loop of the LY S5 sample probably reflects a

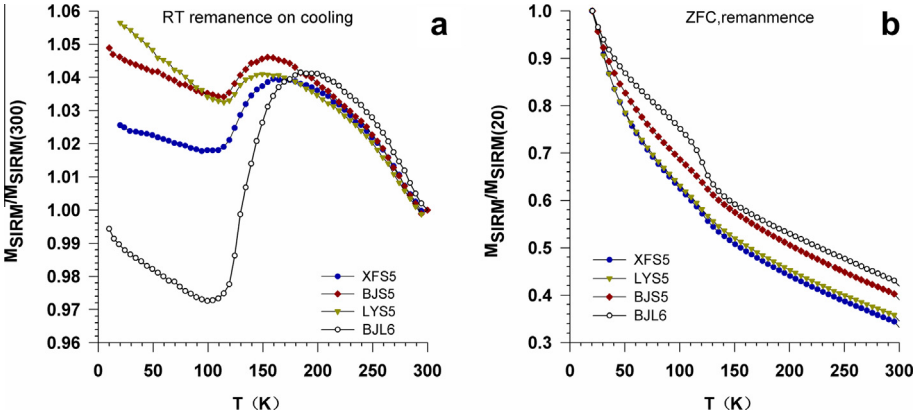

Fig. 3. MPMS measurements in the 20–300 K temperature range. (a) RT-SIRM on cooling from 300 to 20 K and (b) Zero Field Cooled (ZFC) curves of 20 K SIRM from 20 to 300 K. The XFS5, LYS5 and BJ S5 samples were selected from the maximum susceptibility locations of XF, LY and BJ S5-1 unit, the BJL6 is from the parent L6 loess layer of BJ section.

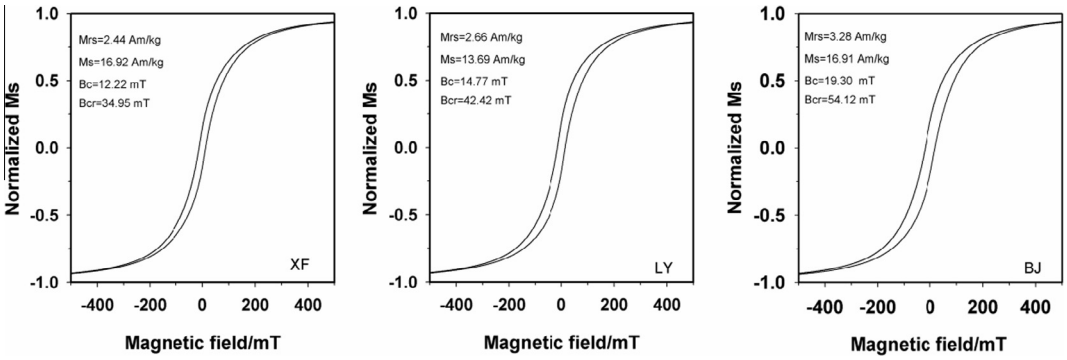

Fig. 4. Hysteresis loops of three magnetic particles separated samples at XF, LY and BJ S5-1 sections.

mixture of magnetic minerals like magnetite/'maghemite' and high coercivity hematite. HIRM data (from 0.025 and 0.063 to 0.107 $Am^2 kg^{-1}$) confirm this interpretation, and so does $S_{300,}$ the best discriminator of antiferromagnetic and ferrimagnetic components (Hesse, 1997). The data show a decline (from 0.98 and 0.95 to 0.93) from XF to BJ. Taken together, comparison of parameters M_{rs}, B_c, B_{cr}, HIRM and S_{300} all suggest that hard magnetic mineral (hematite, goethite) concentrations of S5-1 samples indeed increases from north to south, the direction of rainfall increase.

3.2. Relationship between mineralogical and magnetic properties

Hematite, as estimated from DRS shows clearly positively correlated with χ and χ_{fd} for XF and LY. But it gradually decreases from XF, LY to BJ (Fig. 5a–c and d–f), suggesting that the concentrations of ferrimagnetic magnetite/maghemite and antiferromagnetic hematite produced during pedogenic processes co-exist in paleosols and they increase simultaneously with pedogenic development. Balsam et al. (2004) have also shown that pedogenic ferrimagnetic mineral concentrations were positively correlated with antiferromagnetic hematite in Lingtai and Luochuan loess–paleosol sequences. But the relationships between goethite and χ are different than hematite in the three units (Fig. 5g–i). For XF S5-1 unit (Fig. 5g). Goethite is weakly (R^2 = 0.2804) but positively correlated with χ, which may be interpreted to reflect that SP and/or MD ferrimagnetic minerals (both contributing to χ) and goethite concentration probably increased simultaneously with pedogenic development. For LY S5-1 unit (Fig. 5h), goethite and χ have almost no correlation (R^2 = 0.1202), indicating that goethite concentration changes little with increasing SP and/or MD ferrimagnetic minerals. For BJ S5-1 unit (Fig. 5i), goethite from DRS data is negatively correlated with χ (R^2 = 0.3856), suggesting that goethite concentration increases with reduction in SP ferrimagnetic minerals, meaning that parts of SP ferrimagnetic minerals could have converted to weakly magnetic goethite during pedogenesis in BJ S5-1 unit. The maximum value of hematite + goethite concentrations (with 1.829%, 1.915% and 1.999%, respectively) relatively increases from XF and LY to BJ; this is consistent with discussion of B_c, B_{cr} and HIRM in previous paragraph.

3.3. Geochemical parameters

FeD/FeT can very effectively reveal the chemical weathering degree and/or pedogenesis intensity of paleosols at different levels of soil development (Guo et al., 2000). From Table 2, it is seen that maximum FeD/FeT upon going from XF to LY to BJ are 0.39, 0.41 and 0.42, while FeD% contents are 4.91%, 5.22% and 5.51%, respectively. The concentrations of easily mobile elements such as CaO and Na_2O decrease from XF to LY to BJ while stable elements such as K_2O, Fe_2O_3, Al_2O_3 and Rb concentration increased. All of these features reflect that weathering and leaching degree on one hand

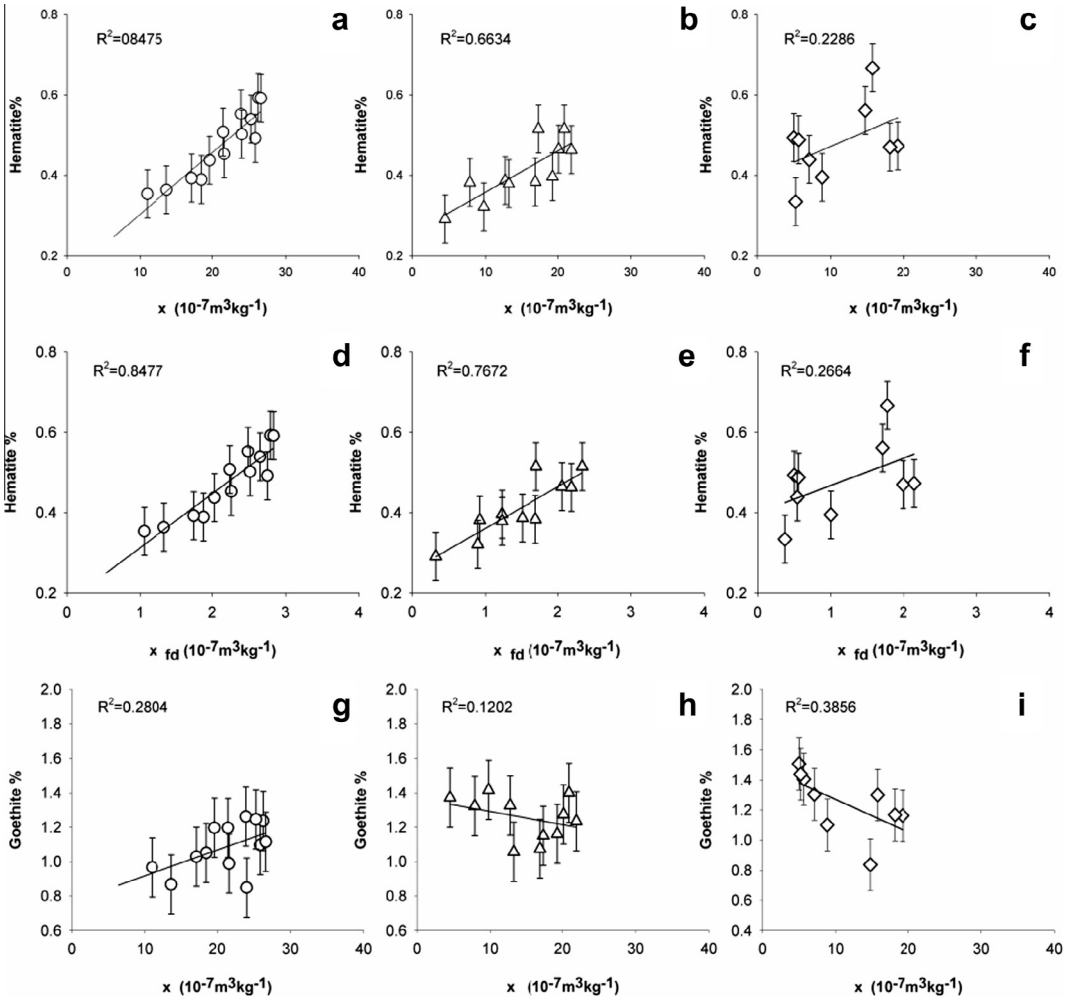

Fig. 5. Correlations between goethite%, hematite% and $\chi_{fd,}$ χ of S5-1 units in XF, LY and BJ sections. The above symbols expressed as (a, d, g) are from Xifeng section; (b, e, h) from Linyou section; (c, f, i) from Baoji section. For hematite estimation, the RMSE is 0.0596, and for goethite estimation RMSE is 0.1714 (Zhang et al., 2009).

Table 2
Geochemical and color parameters.

Section		FeD%	FeD/FeT	Al_2O_3 (wt%)	CaO (wt%)	Na_2O (wt%)	K_2O (wt%)	Rb (ppm)	*a* (%)	*L* (%)
XFS5-1	Min–max	2.05–4.91	0.21–0.39	11.58–14.75	1.31–1.21	1.19–1.80	2.21–3.03	90.5–130.3	6.94–9.17	50.59–58.08
LYS5-1	Min–max	4.13–5.22	0.37–0.41	14.38–15.34	1.01–1.16	1.08–1.26	2.87–3.04	120.5–134.7	7.43–9.06	49.52–56.89
BJ S5-1	Min–max	3.97–5.51	0.35–0.42	14.41–15.5	0.87–1.03	0.83–1.22	2.97–3.16	126.2–137.3	7.91–8.53	46.29–56.80

Fig. 6. The color and iron–manganese cutans of S5-1 paleosol at XF (a), LY (b) and BJ (c) sections. (For interpretation of the references to color in this figure legend, the reader is referred to the web version of this article.)

and pedogenesis intensity on the other of S5-1 paleosols are gradually enhanced from north to south following rainfall increase.

3.4. The color variation of S5-1 paleosols

Previous studies have suggested that post-depositional processes may have changed the loess/paleosol color to a more reddish and darker color than the original eolian dust (Ji et al., 2001; Shen et al., 2006; Sun et al., 2011). '*L*' describes the lightness in color, and is influenced by pedogenic matter. Iron oxides and organic matter darken the loess lightness, whereas carbonate lightens the loess lightness. In contrast, '*a*', which reflects the saturation degree of red, is controlled dominantly by the types and concentrations of iron oxides (especially hematite) (Sun et al., 2011). According to Table 2, '*a*' value rises, while '*L*' value declines (that is redness increases and lightness decreases), indicating that iron oxides (especially hematite) are increasing from XF and LY to BJ. Our field observations revealed that XF S5 paleosol has light red color, with no iron–manganese cutans observed (Fig. 6a). However, the intermediate site of LY S5 paleosol has brown–red color, and can be observed with a few iron–manganese cutans (Fig. 6b). But there are abundant iron–manganese cutans in the BJ S5 paleosol with dark brown–red color (Fig. 6c). Iron–manganese cutans form intermittently between wet and dry periods, under weathering and leaching soil conditions. Weathering destroys iron and manganese silicate minerals or clay minerals to release Fe, Mn, etc. under moist over-saturated soil conditions. Also, iron and manganese oxides are destroyed, releasing Fe^{2+} and Mn^{2+} which migrate with water into the soil surface, which then oxidizes in dry climatic conditions and form iron–manganese oxide (Huang et al., 2008). The redness, lightness and field observations all reflect the increase of iron oxides (especially hematite and/or goethite) upon going from XF and LY to BJ. Thus geochemical and color data support inferences based on magnetic parameters.

4. Disscussion and conclusion

As is well-known, χ is a useful palaeoclimatic indicator in the central CLP. At Xifeng (Liu et al., 2001), Lingtai (Ding et al., 1998) and Linyou profiles, the S5-1 layer has the highest χ value in the whole profile. In combination with pedogenic study (An et al., 1987), this indicates that S5-1 is the most developed paleosol. However, the χ value of Baoji S5-1 horizon is low within the profile, and also lower than S5-1 horizon at XF and LY profiles (Fig. 2 and Table 1). The MAP values (Fig. 1) and MAT values generally increase from XF to BJ, meaning increasing pedogenic condition, but the χ value of S5-1 paleosol unit is declining (Fig. 2a) with pedogenesis. Paleosols S5-1 at the three sections will now be compared overall to analyze for the possible reasons.

The ratios of FeD/FeT, FeD%, elements of Al_2O_3, K_2O, Rb, CaO, Na_2O concentrations, and redness values (Table 2), all show that S5-1 paleosol's weathering intensity does strengthen from north to south. Hao and Guo (2005) studied loess–paleosol pedogenesis intensity using FeD/FeT data to confirm that paleosol chemical weathering intensity was higher in the south of CLP than in the north, leading to a significantly increasing trend from north to south. Low-temperature magnetic curves have already shown that the degree of maghemitization increases on going from loess to paleosol in a single section and also from XF, LY to BJ (Fig. 3). The increased ferrimagnetic component was mainly oxidized magnetite, it was the major contributor to remanence. These further confirm that χ decreases from paleosols S5-1, north to south, and is caused by attendant strong pedogenesis. This is also a typical feature of Tertiary red clays, where low χ contrasts with increase in chemical indicator of pedogenesis (Ding et al., 2001).

According to the correlation between hematite, goethite, χ and χ_{fd} (Fig. 5), we found that with increasing pedogenic degree, both hematite and other pedogenic ferrimagnetic mineral concentrations increased in the three S5-1 paleosol layers. Therefore, we speculate that either only a small fraction of ferrimagnetic minerals transformed into goethite, but some goethite transformed into hematite with environmental aridity in LY S5-1 paleosol layer, and part of the ferrimagnetic minerals transformed into goethite in BJ S5-1 paleosol layer. In the field, we also observed (Sections 3 and 4) no Fe–Mn films were seen in XF S5 paleosol layer (Fig. 6a), and only a little amount of Fe–Mn films in LY S5 paleosol layer (Fig. 6b), and abundant Fe–Mn films in BJ S5 paleosol layer (Fig. 6c). This is consistent with the higher goethite% and B_{cr} (Fig. 4). Therefore, the pedogenic ferrimagnetic mineral concentration decreases spatially from north to south, and the total concentration of goethite + hematite and goethite both increase, which will increase the contribution to remanence HIRM.

The parameters of, χ_{ARM} and χ_{ARM}/SIRM rise from XF to LY, then decrease from LY to BJ (Fig. 2d, e and Table 1), showing that SD ferrimagnetic particles increased from XF to LY, but decreased on going from LY to BJ. χ_{fd} declined from XF to BJ. Low temperature ZFC remanence curves indicated that the grain sizes of three

paleosol samples was finer with more SP grains than in loess L6. SP % was nearly equal at XF and LY samples, but higher than in the BJ sample. The contribution of SP (at 300 K) grains to remanence (at 10 K) only slightly decreases from XF, LY to BJ. It was the loss SP and SSD ferrimagnetic particles that have caused reduction of χ_{fd}, χ_{ARM}, χ_{ARM}/SIRM and χ_{fd}/χ_{ARM} values. This observation is compatible with magnetite dissolution, which is expected to selectively eliminate first the smaller grain sizes (Smirnov and Tarduao, 2000).

In summary, the degree of pedogenesis of S5-1 paleosol increased from XF to LY to BJ, ferrimagnetic minerals (mainly oxidized magnetite or maghemite) concentrations reduced, and total concentrations of antiferromagnetic minerals (goethite and hematite) gradually increased. The SP particles decreased and SSD ferrimagnetic particles initially increased from XF to LY, but then reduced from LY to BJ, the highest rainfall site. The reason for this phenomenon may be related with soil effective rainfall. Orgeira et al. (2011) proposed that soil water balance, rather than MAP, is the most important factor that controls magnetic enhancement because it dominate the annual soil 'wetting' and 'drying' cycle. They constructed a quantitative model for the climatic dependence of magnetic enhancement in loessic soils. In the central and northern CLP, such as Xifeng (Liu et al., 2001) and Lingtai (Ding et al., 1998) sections, MAR are less than 550 mm, and according to the meteorological data based on last 30 years, MAR-PET (potential evapotranspiration) < 0. Under aerobic oxidizing conditions, with increasing weathering degree, hydrolysis of primary Fe minerals release Fe^{2+} ions, whose oxidation results in the production of poorly crystallized ferrihydrite, ferrihydrite oxidized into maghemite and hematite. The pedogenic maghemite concentrations increased under aerobic conditions which led to a generally positive correlation between magnetic enhancement and pedogenesis as is generally found. Therefore, the susceptibility of the paleosol unit S5-1 is the highest at these two sections in the central and northern CLP (Ding et al., 1998; Balsam et al., 2004).

However, from XF to LY to BJ, modern mean annual rainfall (which was 550, 680 and 720 mm, Fig. 1) increases from the central to southern of CLP. Since the S5-1 horizon is the most prominent and well-developed paleosol in the CLP. Paleosol S5-1 period (within S5 sub-period) represents very warm and more humid climate for the past 2.5 Ma (An et al., 1987). Rainfall was more than modern values, and the rainfall mainly occurred from July to September. Also, the meteorological data based on last 30 years show the difference between the maximum rainfall during heavy rainfall and mean annual evapotranspiration for last 30 years is −37, −20 and 241 mm, respectively, from XF, LY to BJ. Thus the effective moisture increases. Especially at BJ, where MAR-PET > 0. Thus periodic heavy rainfall can make soil oversaturated with moisture, which may lower the pH value and cause dissolution of Fe^{2+} ions in the crystal lattice, whose oxidation results in the production of ferrihydrite, and which can be further evolved into maghemite or hydro-maghemite with grain size growing from SP to SD before its transformation into hematite (Liu et al., 2008; Michel et al., 2010; Barrón et al., 2012). The new hematite can also form independently from ferrihydrite during high rainfall (Cornell and Schwertmann, 2003). This provides further evidence on the pathway of ferrihydrite → maghemite-like phase → hematite (Hu et al., 2013; Barrón and Torrent, 2002). During more wet soil condition, Fe^{2+} which migrates with water into the soil surface can form weakly magnetic goethite etc (Huang et al., 2008). Therefore, the magnetic enhancement declines from XF to LY to BJ. This further demonstrates the efficacy of the model proposed by Orgeira et al. (2011).

Modern soil studies show that magnetic susceptibility increases with increasing pedogenic degree in aerobic soil with low and moderate rainfall. However, when the moisture is high, the susceptibility decreases (Maher and Thompson, 1994; Han et al., 1996; Balsam et al., 2011; Long et al., 2011). In the vermiculated red soil in southern China, pedogenic maghemite has dissolved into the white veins under long-term water logging conditions and transformation of highly magnetic maghemite to weakly magnetic hematite, has occurred causing a significant decrease in susceptibility (Hu et al., 2009; Liu et al., 2012; Wang et al., 2013). Many scholars (Maher, 1998; Cornell and Schwertmann, 2003; Liu et al., 2008; Bábek et al., 2011) have reported that pedogenic fine maghemite and/or magnetite are reductively dissolved in anaerobic soil conditions, causing the depletion of soil magnetism.

Now we can make a few conclusions from the above research: The rock magnetic and geochemistry parameters show that upon going from XF to BJ via LY pedogenic ferrimagnetic mineral (mainly oxidized magnetite or maghemite) concentrations are decreasing, and the antiferromagnetic mineral (hematite and goethite) concentrations are relatively increased. Fine-grained maghemite was the main contributor to magnetic enhancement parameters.

The maghemite and hematite concentration appears to increase simultaneously with increasing pedogenic degree in S5-1 sub-palaeosol horizon (Fig. 5d–f), thus in that specific aspect being similar to soil in arid regions of SW Spain. We find that weathering of the Fe-bearing minerals had resulted in the neoformation of hematite and maghemite, but the estimated goethite concentration shows irregular but increasing trend from north to south. The relationship between goethite and maghemite concentrations at each horizon is therefore unclear.

The Fe–Mn cutans in the S5 paleosol increase from XF to BJ, which was caused by the change in composition of the iron minerals. In the XF-BJ transact more and more fine-grained SP and SSD sized strongly magnetic minerals (mainly oxidized magnetite and maghemite) were converted later into weakly magnetic minerals (mainly hematite and goethite) during pedogenesis, which caused the currently observed decrease of susceptibility for palaeosol S5-1 sub-units from XF to LY to BJ.

Acknowledgements

We thank Prof. Subir K. Banerjee of the IRM, who checked the English and revised the ideas expressed in the whole manuscript carefully. The MPMS and VSM measurements were made at the Institute for Rock Magnetism (IRM), University of Minnesota. We thank Mike Jackson, Peat Sølheid and Dario Bilardello for their help with the experiments, and thank Prof. W.G. Zhang and Y. Dong Ph. D., State Key Laboratory of Estuarine and Coastal Research, East China Normal University, for their help with the DRS measurements. This research was supported by the Natural Science Foundation of China (41202129, 51574014, 41072124, 41210002 and 41402149), Shengjun Miao was further supported by National Key Basic Research Program of China (973 Program) (2015CB060200) and Xuelian Guo was further supported by the China Scholarship Council (201406185002). The IRM is supported by United States National Foundations EAR/IF division and the University of Minnesota. This is IRM contribution no.1501. We are grateful to two anonymous reviewers for their helpful suggestions.

References

An, Z.S., Liu, T.S., Zhu, Y.Z., Sun, F., 1987. The paleosol complex S5 in the China Loess Plateau – a record of climatic optimum during the last 1.2 Ma. Geojournal 15, 141–143.

Bábek, O., Chlachula, J., Grygar Matys, T.M., 2011. Non-magnetic indicators of pedogenesis related to loess magnetic enhancement and depletion: examples from the Czech Republic and southern Siberia. Q. Sci. Rev. 30, 967–979.

Balsam, W., Ji, J.F., Chen, J., 2004. Climatic interpretation of the Luochuan and Lingtai loess sections, China, based on changing iron oxide mineralogy and magnetic susceptibility. Earth Planet. Sci. Lett. 223, 335–348.

Balsam, W.L., Ellwood, B.B., Ji, J.F., Williams, E.R., Long, X.Y., Hassani, A.E., 2011. Magnetic susceptibility as a proxy for rainfall: worldwide data from tropical and temperate climate. Q. Sci. Rev. 30, 2732–2744.
Banerjee, S.K., King, J., Marvin, J., 1981. A rapid method for magnetic granulometry with applications to environmental studies. Geophys. Res. Lett. 8, 333–336.
Banerjee, S.K., Hunt, C.P., Liu, X.M., 1993. Separation of local signals from the regional paleomonsoon record of the Chinese Loess Plateau: a rock-magnetic approach. Geophys. Res. Lett. 20 (9), 843–846.
Barrón, V., Torrent, J., 2002. Evidence for a simple pathway to maghemite in Earth and Mars soils. Geochim. Cosmochim. Acta 66, 2801–2806.
Barrón, V., Torrent, J., Michel, F.M., 2012. Critical evaluation of the revised akdalaite model for ferrihydrite – discussion. Am. Mineral. 97, 253–254.
Begét, J., Stone, D., Hawkins, D., 1990. Paleoclimate forcing of magnetic susceptibility variations in Alaskan loess. Geology 18, 40–43.
Chlachula, J., 2003. The Siberian loess record and its significance for reconstruction of Pleistocene climate change in north-central Asia. Q. Sci. Rev. 22, 1879–1906.
Cornell, R.M., Schwertmann, U., 2003. The Iron Oxides: Structure, Properties, Reactions, Occurrences and Uses. Wiley-VCH, Weinheim, Germany.
Deng, C.L., Zhu, R.X., Jackson, M.J., Verosub, K.L., Singer, M.J., 2001. Variability of the temperature-dependent susceptibility of the Holocene eolian deposits in the Chinese Loess Plateau: a pedogenesis indicator. Phys. Chem. Earth A 26 (11–12), 873–878.
Ding, Z.L., Sun, J.M., Yang, S.L., Liu, T.S., 1998. Preliminary magnetostratigraphy of a thick eolian red clay-loess sequence at Lingtai, the Chinese Loess Plateau. Geophys. Res. Lett. 25, 1225–1228.
Ding, Z.L., Yang, S.L., Sun, J.M., Liu, T.S., 2001. Iron geochemistry of loess and red clay deposits in the Chinese Loess Plateau and implications for long-term Asian monsoon evolution in the last 7.0 Ma. Earth Planet. Sci. Lett. 185, 99–109.
Evans, M.E., Heller, F., 2003. Environmental Magnetism: Principles and Applications of Enviromagnetics. Academic Press, New York, pp. 1–299.
Evans, M.E., Rutter, N.W., Catto, N., Chlachula, J., Nyvlt, D., 2003. Magnetoclimatology: teleconnection between the Siberian loess record and North Atlantic Heinrich events. Geology 31, 537–540.
Fine, P., Verosub, K.L., Singer, M.J., 1995. Pedogenic and lithogenic contributions to the magnetic susceptibility record of the Chinese loess/paleosol sequence. Geophys. J. Int. 122, 97–107.
Fischer, H., Luster, J., Gehring, A.U., 2008. Magnetite weathering in a vertisol with seasonal redox-dynamics. Geoderma 143, 41–48.
Geiss, C.E., Zanner, C.W., 2006. How abundant is pedogenic magnetite? Abundance and grain size estimates for loessic soils based on rock magnetic analyses. J. Geophys. Res. 111, B12S21. http://dx.doi.org/10.1029/2006JB004564.
Guo, Z.T., Biscaye, P., Wei, L.Y., Chen, X.F., Peng, S.Z., Liu, T.S., 2000. Summer monsoon variations over the last 1.2 Ma from the weathering of loess-soil sequences in China. Geophys. Res. Lett. 27 (12), 1751–1754.
Guo, X.L., Liu, X.M., Lü, B., Tang, D.P., Mao, X.G., Chen, J.S., Chen, X.Y., 2011. Comparison of topsoil magnetic properties between the loess region in Tianshan Mountains and Loess Plateau, China, and its environmental significance. Chin. J. Geophys. 54, 485–495.
Guo, X.L., Liu, X.M., Li, P.Y., Lü, B., Guo, H., Chen, Q., Ma, M.M., 2013. The magnetic mechanism of paleosol S5 in the Baoji section of the southern Chinese Loess Plateau. Q. Int. 306, 129–136.
Han, J.M., Lü, H.Y., Wu, N.Q., 1996. Magnetic susceptibility of modern soils in China and climate conditions. Stud. Geophys. Geod. 40, 262–275.
Hanesch, M., Scholger, R., 2005. The influence of soil type on the magnetic susceptibility measured throughout soil profiles. Geophys. J. Int. 161, 50–56.
Hao, Q.Z., Guo, Z.T., 2005. Spatial variations of magnetic susceptibility of Chinese loess for the last 600 kyr: implications for monsoon evolution. J. Geophys. Res. 110, B12101. http://dx.doi.org/10.1029/2005JB003765.
Heller, F., Shen, C.D., Beer, J., Liu, X.M., Liu, T.S., Bronger, A., Suter, M., Bonani, G., 1993. Quantitative estimates of pedogenic ferromagnetic mineral formation in Chinese loess and palaeoclimatic implications. Earth Planet. Sci. Lett. 114, 385–390.
Hesse, P.P., 1997. Mineral magnetic 'tracing' of aeolian dust in southwest Pacific sediments. Palaeogeogr. Palaeoclimatol. Palaeoecol. 131, 327–353.
Hu, X.F., Wei, J., Xu, L.F., Zhang, G.L., Zhang, W.G., 2009. Magnetic susceptibility of the quaternary red clay in subtropical China and its paleoenvironmental implications. Palaeogeogr. Palaeoclimatol. Palaeoecol. 279, 216–232.
Hu, P.X., Liu, Q.S., Torrent, J., Barrón, V., Jin, C.S., 2013. Characterizing and quantifying iron oxides in Chinese loess/paleosols: implications for pedogenesis. Earth Planet. Sci. Lett. 369–370, 271–283.
Huang, L., Hong, J., Tan, W.F., Hu, H.Q., Liu, F., Wang, M.K., 2008. Characteristics of micromorphology and element distribution of iron–manganese argillans in typical soils of subtropical China. Geoderma 146, 40–47.
Hunt, C.P., Banerjee, S.K., Han, J.M., Solheid, P.A., Oches, E., Sun, W.W., Liu, T.S., 1995. Rock magnetic proxies of climate change in the loess-paleosol sequences of the western Loess Plateau of China. Geophys. J. Int. 123, 232–244.
Ji, J.F., Balsam, W., Chen, J., 2001. Mineralogic and climatic interpretations of the Luochuan loess section (China) based on diffuse reflectance spectrophotometry. Q. Res. 56, 23–30.
Kalm, V.E., Rutter, N.W., Rokosh, C.D., 1996. Clay minerals and their paleoenvironmental interpretation in the Baoji loess section, Southern Loess Plateau, China. Catena 27, 49–61.
King, J., Banerjee, S.K., Marvin, J., Ozdemir, O., 1982. A comparison of different magnetic methods for determining the relative grain size of magnetite in natural materials: some results from lake sediments. Earth Planet. Sci. Lett. 59, 404–419.
Kravchinsky, V.A., Zykina, V.S., Zykin, V.S., 2008. Magnetic indicators of global paleoclimate cycles in Siberian loess-paleosol sequences. Earth Planet. Sci. Lett. 265, 498–514.
Lagroix, F., Banerjee, S.K., 2004. The regional and temporal significance of primary aeolian magnetic fabrics preserved in Alaskan loess. Earth Planet. Sci. Lett. 225, 379–395.
Liu, X.M., Rolph, T., Bloemendal, J., Shaw, J., Liu, T.S., 1995. Quantitative estimates of paleoprecipitation at Xifeng in the loess plateau of China. Palaeogeogr. Palaeoclimatol. Palaeoecol. 113, 243–248.
Liu, X.M., An, Z.S., Qiang, X.K., Hesse, P., Lu, H.Y., Zhou, J., Cai, Y.J., Rolph, T., Hesse, P., 2001. Magnetic properties of the Tertiary red clay from Gansu Province, China and its paleoclimatic significance. Sci. China Earth Sci. 44, 635–651.
Liu, Q.S., Jackson, M.J., Yu, Y.Z., Chen, F.H., Deng, C.L., Zhu, R.X., 2004. Grain size distribution of pedogenic magnetic particles in Chinese loess/paleosols. Geophys. Res. Lett. 31, L22603. http://dx.doi.org/10.1029/2004gl021090.
Liu, Q.S., Torrent, J., Maher, B.A., Yu, Y.J., Deng, C.L., Zhu, R.X., Zhao, X.X., 2005. Quantifying grain size distribution of pedogenic magnetic particles in Chinese loess and its significance for pedogenesis. J. Geophys. Res. 110, B11102. http://dx.doi.org/10.1029/2005JB 003726.
Liu, Q.S., Deng, C.L., Torrent, J., Zhu, R.X., 2007. Review of recent developments in mineral magnetism of the Chinese loess. Q. Sci. Rev. 26, 368–385.
Liu, Q.S., Barrón, V., Torrent, J., Eeckhout, S.G., Deng, C.L., 2008. Magnetism of intermediate hydromaghemite in the transformation of 2-line ferrihydrite into hematite and its paleoenvironmental implications. J. Geophys. Res. 113, B01103. http://dx.doi.org/10.1029/2007jb005207.
Liu, C.C., Deng, C.L., Liu, Q.S., 2012. Mineral magnetic studies of the vermiculated red soils in southeast China and their paleoclimatic significance. Palaeogeogr. Palaeoclimatol. Palaeoecol. 329–330, 173–183.
Long, X.Y., Ji, J.F., Balsam, W., 2011. Rainfall-dependent transformations of iron oxides in a tropical saprolite transect Hainan Island, South China: spectral and magnetic measurements. J. Geophys. Res. 116. http://dx.doi.org/10.1029/2010JF0 01712.
Maher, B.A., 1998. Magnetic properties of modern soils and quaternary loessic paleosols: paleo-climatic implications. Palaeogeogr. Palaeoclimatol. Palaeoecol. 137, 25–54.
Maher, B.A., Thompson, R., 1994. Comments on: pedogenesis and paleoclimate-interpretation of the magnetic susceptibility record of Chinese loess-paleosol sequences. Geology 23, 857–858.
Maher, B.A., Alekseev, A., Alekseeva, T., 2003. Variation of soil magnetism across the Russian steppe: its significance for use of soil magnetism as a palaeorainfall proxy. Q. Sci. Rev. 21, 1571–1576.
Michel, F.M., Barrón, V., Torrent, J., Morales, M.P., Serna, C.J., Boily, J.F., Liu, Q.S., Ambrosini, A., Cismasu, A.C., Brown, G.E., 2010. Ordered ferrimagnetic form of ferrihydrite reveals links among structure, composition, and magnetism. Proc. Natl. Acad. Sci. U.S.A. 107, 2787–2792.
Nie, J.S., Song, Y.G., King, J.W., Fang, X.M., Heil, C., 2010. HIRM variations in the Chinese red-clay sequence: insights into pedogenesis in the dust source area. J. Asian Earth Sci. 38, 96–104.
Orgeira, M.J., Egli, R., Compagnucci, R.H., 2011. A quantitative model of magnetic enhancement in loessic soils. In: Petrovský, E., Ivers, D., Harinarayana, T., Herrero-Bervera, E. (Eds.), The Earth's Magnetic Interior. Springer, Netherlands, pp. 361–397.
Özdemir, Ö., Dunlop, D.J., 2010. Hallmarks of maghemitization in low-temperature remanence cycling of partially oxidized magnetite nanoparticles. J. Geophys. Res. 115, B02101. http://dx.doi.org/10.1029/2009JB006756.
Porter, S.C., Hallet, B., Wu, X.H., 2001. Dependence of near surface magnetic susceptibility on dust accumulation rate and precipitation on the Chinese Loess Plateau. Q. Res. 55 (3), 271–283.
Qiang, X.K., An, Z.S., Li, H.M., Chang, H., Song, Y.G., 2005. Magnetic properties of Jiaxian red clay sequences from northern Chinese Loess Plateau and its paleoclimatic significance. Sci. China Earth Sci. 48, 1234–1245.
Scheinost, A.C., Chavernas, A., Barrón, V., Torrent, J., 1998. Use and limitations of second-derivative diffuse reflectance spectroscopy in the visible to near-infrared range to identify and quantify Fe oxide minerals in soils. Clays Clay Miner. 46, 528–536.
Shen, Z.X., Cao, J.J., Zhang, X.Y., Arimoto, R., Ji, J.F., Balsam, W.L., Wang, Y.Q., Zhang, R. J., Li, X.X., 2006. Spectroscopic analysis of iron-oxide minerals in aerosol particles from northern China. Sci. Total Environ. 367, 899–907.
Smirnov, A.V., Tarduao, J.A., 2000. Low-temperature magnetic properties of pelagic sediments (Ocean Drilling Program site 805C): tracers of magnemitization and magnetic mineral reduction. J. Geophys. Res. 105, 16457–16471.
Song, Y.G., Shi, Z.T., Fang, X.M., Nie, J.S., Naoto, I., Qiang, X.K., Wang, X.L., 2010. Loess magnetic properties in the Ili Basin and their correlation with the Chinese Loess Plateau. Sci. China Earth Sci. 53, 419–431.
Spassov, S., Heller, F., Kretzschmar, R., Evans, M.E., Yue, L.P., Nourgaliev, D.K., 2003. Detrital and pedogenic magnetic mineral phases in the loess/palaeosol sequence at Lingtai (central Chinese Loess Plateau). Phys. Earth Planet. Inter. 140, 255–275.
Sun, Y.B., He, L., Liang, L.J., An, Z.S., 2011. Changing color of Chinese loess: geochemical constraint and paleoclimatic significance. J. Asian Earth Sci. 40, 1131–1138.
Taylor, S., Lagroix, F., 2014. Mineral magnetic analysis of the upper pleniglacial loess-paleosol deposits from Nussloch loess sequence (Germany): an insight into local environmental processes. Geophys. J. Int. 199, 1463–1480.
Torrent, J., Liu, Q.S., Bloemendal, J., Barrón, V., 2007. Magnetic enhancement and iron oxides in the upper Luochuan loess–paleosol sequence, Chinese Loess Plateau. Soil Sci. Soc. Am. J. 71, 1570–1578.

Torrent, J., Liu, Q.S., Barrón, V., 2010. Magnetic minerals in Calcic Luvisols (Chromic) developed in a warm Mediterranean region of Spain: origin and paleoenvironmental significance. Geoderma 154, 465–472.

Wang, S.Y., Lin, S., Lu, S.G., 2013. Rock magnetism, iron oxide mineralogy and geochemistry of Quaternary red earth in central China and their paleopedogenic implication. Palaeogeogr. Palaeoclimatol. Palaeoecol. 379–380, 95–103.

Willimas, M.A.J., Dunkerley, D.L., Deckker, Kershew, A.P., Stokes, T.J., 1993. Quaternary Environments. Edwards Arnold (Publishers) Ltd.

Worm, H.U., 1998. On the superparamagnetic-stable single domain transition for magnetite, and frequency dependence of susceptibility. Geophys. J. Int. 133, 201–206.

Xie, Q.Q., Chen, T.H., Xu, H.F., Chen, J., Ji, J.F., Lu, H.Y., Wang, X.Y., 2009. Quantifying the contribution of pedogenic magnetic minerals to magnetic susceptibility of loess and paleosols on Chinese Loess Plateau: paleoclimatic implication. J. Geophys. Res. 114 (B9). http://dx.doi.org/10.1029/2008JB005968.

Zhang, W.G., Yu, L.Z., Lu, M., Zheng, X.M., Ji, J.F., Zhou, L.M., Wang, X.Y., 2009. East Asian summer monsoon intensity inferred from iron oxide mineralogy in the Xiashu Loess in southern China. Q. Sci. Rev. 28, 345–353.

Zhang, W.G., Dong, C.Y., Ye, L.P., Yu, L.Z., 2012. Magnetic properties of coastal loess on the Midao islands, northern China: implications for provenance and weathering intensity. Palaeogeogr. Palaeoclimatol. Palaeoecol. 333–334, 150–167.

Zhao, J.B., Cao, J.J., Jin, Z.D., Xing, S., Shao, T.J., 2013. The fifth paleosol layer in the southern part of China's Loess plateau and its environmental significance. Q. Int. http://dx.doi.org/10.1016/j.quaint.2012.12.044.

Zhou, L.P., Oldfield, F., Wintle, A.G., Robinson, S.G., Wang, J.T., 1990. Partly pedogenic origin of magnetic variations in Chinese loess. Nature 346, 737–739.